



## Discovery of novel quaternary bulk metallic glasses using a developed correlation-based neural network approach



Majid Samavatian<sup>a,\*</sup>, Reza Gholamipour<sup>a</sup>, Vahid Samavatian<sup>b</sup>

<sup>a</sup> Department of Advanced Materials and Renewable Energy, Iranian Research Organization for Science and Technology (IROST), Tehran 3313193685, Iran

<sup>b</sup> Department of Electrical Engineering, Sharif University of Technology, 68260 Tehran, Iran

### ARTICLE INFO

#### Keywords:

Neural network  
Bulk metallic glass  
Glass forming ability  
Materials design

### ABSTRACT

The immense space of composition-processing parameters leads to numerous trial-and-error experimental works for engineering of novel bulk metallic glasses (BMGs). To tackle this challenging problem, it is required to consider specific guidelines which are able to restrict the productive alloying compositions. In this work, a correlation-based neural network (CBNN) approach was developed, based on a dataset of 7950 alloying compositions, to design potential new MGs through prediction of casting ability, reduced glass transition ( $T_{rg}$ ) and critical thickness ( $D_{max}$ ). This approach involves individual and mutual characteristics of contributory factors to improve the prediction accuracy. To validate our model, we selected the ZrCoAl alloying system and investigated the microalloying effects on the glass forming possibility (GFP). According to the results, the microalloying process effects strongly depended on the inherent features of added element. Moreover, the CBNN model predicted a quaternary system, i.e. ZrCoAlNi, in which the high GFP area was extended through a wide range of chemical compositions. Finally, it is concluded that the established framework offers a roadmap for potential applications in the development of new quaternary MG alloys.

### 1. Introduction

Bulk metallic glasses (BMGs) are structurally amorphous solids lacking the crystalline long-range order. Although the unique atomic structure of BMGs leads to superior physical and mechanical properties, designing novel amorphous materials with widespread engineering applications seems strenuous [1–4]. Predominantly, the individual kinetic nature of transition from liquid to solid in BMGs suggests that multiple processing parameters influence their glass forming ability (GFA). Hence, time-consuming experimentations are needed to cover the space of composition-processing parameters for the BMG design. To mitigate this problem, researchers proposed several empirical and physical models based on topological arrangement [5], thermodynamics [6–8], atomic size mismatches [9], valence electron distribution [10], atomic number fraction [11], near deep eutectic composition [12] and etc. to overcome the challenge of trial-and-error experimental works for the BMGs design. Nevertheless, the mentioned models are proper for certain chemical compositions so that there is no thorough-paced approach to reliably predict a vast range of new glassy formers.

In recent years, artificial intelligence (AI) has been employed to develop predictive tools for materials design [13]. Fracture mechanism

of materials [14–16], phase transformation analysis [17–19], microstructure recognition [20–22], material structure–property linkage [23–25] and materials degradation [26] are the examples of AI applications in materials science. In the meanwhile, few works have been additionally executed to engineer the novel MGs through the AI approaches. For instance, Majid et al [27] reported that general regression neural network can accurately predict the GFA in the BMGs; however, their work lacked sufficient input data and ignored thermodynamic aspect of BMGs. Tripathi et al [28,29] developed a statistical learning model to express the GFA in terms of the basic components related to the generic attribute of the compositional elements. Using a vector classification method, Sun et al [30] found that the liquidus temperature fulfills a key role in the prediction of GFA for binary amorphous alloys. Ward et al [31] developed a predictive model which accurately evaluated the possible critical casting diameter and super-cooled liquid temperature in the BMGs by providing a massive database of MG experiments. A combined iterative machine learning (ML) and high-throughput experiments was another proposed approach leading to the accelerated detection of new MGs [32]. Cai et al [33] established a radial base function artificial neural network which was able to accurately estimate the undercooled liquid region in glassy alloys. With this predictive model, a group of ZrAlNiCu MGs with certain critical cooling

\* Corresponding author.

E-mail address: [m.samavatian@srbiau.ac.ir](mailto:m.samavatian@srbiau.ac.ir) (M. Samavatian).

rate and optimum dimensions was designed [34,35]. Moreover, other features of MGs such as elastic moduli, softness and structural heterogeneity were recently evaluated by ML approaches [36–40]. The consistent findings of these all studies indicate the capability of constructing predictive models with no deficiencies typically lied in the conventional empirical rules and physical approaches. However, there seems to be a long open way to employ all the potential of computational intelligence for designing of novel glassy alloys. Hence, this paper firstly aims to introduce a novel correlation-based neural network (CBNN) approach for advancing the design and comprehensive evaluation of BMGs with innumerable chemical compositions. The CBNN approach considered contributory factors and their mutual relations to predict the GFA and the critical casting diameters of BMGs. Secondly, we validate our CBNN approach by developing new quaternary BMGs and show that how a ternary BMG can be modified with a microalloying process.

## 2. A paradigm shift from conventional ML to CBNN approach

As mentioned in section 1, artificial intelligence is an efficient approach for predicting the inherent characteristics of the glassy alloys. In the meanwhile, the established model should be consistent with the input features and their impacts on the outcome. For this reason, the researchers have tried to shift from the conventional models to the novel machine learned approaches, which are efficient in materials prediction, especially glassy alloys. As an illustration, Tripathi et al [29] constructed their learning model based on generic features of constituents and their quantitative presence in an alloying composition. In another work, in the case of MGs it was reported that the radial base function artificial neural network improved the approximation, learning rate, and sorting capacity [33]. According to the established approach by Ren et al [32], the high-throughput experiments and ML model can be simultaneously applied in a feedback/iterative loop to speed up the MG prediction. In our case, a crucial aspect, namely the dependencies and correlations of the input features and their effects on the outcome, is under our meticulous attention. By considering these correlations, two significant benefits are achieved. First of all, the spent time for training the network considerably declines, which allows us to employ deeper networks in comparison with the conventional AI approaches. Secondly, one can achieve a dramatic increase in the accuracy of the predictions owing to the consideration of the input features correlations. Thus, our proposed correlation based neural network model overcomes the deficiencies which conventional ML are suffering from.

## 3. Materials and methods

### 3.1. Preliminary preparation for neural network modeling

As given in Fig. 1, the cognitive process for constructing a neural network model is divided into the several sequential steps. At the first step, the associated data were carefully collected from publicly reliable resources. Thanks to Landolt-Bornstein Handbook with a huge number of ternary amorphous alloys information [41], we also considered the dataset recorded by Logan Ward [42] on Citrination website. Moreover, our resource was updated by collecting new data from papers published in recent years [43–64]. The casting capability of amorphous alloys, glass transition temperature ( $T_g$ ), melting temperature ( $T_l$ ) and maximum casting thickness ( $D_{max}$ ) are items recorded from mentioned resources. In general, a database of 7,950 MG experiments was generated for the neural network modeling (see [Supplementary one](#)). At the second step, it is crucial to process data according to the input and output items in the model. While the chemical compositions of alloys are described as the input data, we look for the parameters like GFA and maximum casting thickness as the indicators of promising alloys. We firstly classified our dataset somehow to indicate whether the alloys can

form BMG, MG ribbon or crystalline type. The maximum casting thickness ( $D_{max}$ ) was another dataset prepared for the learning model. The  $D_{max}$  for BMGs was considered as the critical casting diameter, while 0.15 and 0 mm critical casting thicknesses were allocated to the MG ribbons and the crystalline alloys, respectively. With the presence of several thickness sizes for an individual alloy composition, we assumed the maximum one. There are several indicators for GFA analysis. However, many of these indicators comprise  $T_g$ ,  $T_x$  and  $T_l$  altogether. On the other side, there are few glassy compositions in data resource, which include these thermal characteristics. For this reason, the selection of GFA indicator is limited to simple criteria such as reduced glass transition temperature ( $T_{rg}$ ), in which the criterion is just derived from  $T_g$  and  $T_l$ , while it remains a reliable parameter for GFA evaluation. Hence, we classified  $T_g$  and  $T_l$  to quantitatively estimate the GFA for the predicted compositions. The 721 entries were collected from the literature for this specific purpose. It is worth-mentioning that the average values were considered for the unique alloy compositions with multiple controversy reports.

At the third step, an adequate set of attributes was determined for target outputs to achieve a well-working neural network process. In general, there are inherent features for each constituent in an alloying composition defining the eventual properties of the material. Hence, it is crucial to correlate these features somehow to differentiate each alloying composition based on physical factors. There are multiple correlated attributes affecting the casting capability of MG materials and defining the GFA. These attributes are divided into distinct sub-categories, while they retain their correlations to each other. The inherent elemental properties, valence electron distribution, thermodynamic and kinetic parameters are major subcategories generally related to the glass formation [37]. The inherent characteristics of elements including atomic fundamental properties, physical and chemical features comprise basic items influencing the ultimate properties of a glassy alloy. Hence, the inherent characteristics of elements, which show the known empirical rules for glass formation [31], are the main primary attributes considered for data processing and representation. These attributes are given in [Table S1 supplementary two](#). The linear mixture rule was employed to calculate the alloy attributes from the corresponding inherent elemental attributes. The thermodynamic parameters are also paramount of important in evolution of a glassy alloy. In fact, the GFA is significantly correlated to the thermodynamics, in which the possible atomic arrangement of atoms to create a glassy structure is considered. Mixing enthalpy, normalized mixing entropy [37] and Gibbs free energy of mixing [8] are known attributes applied in our model. Moreover, in this work the viscosity parameter [65,66] comes into play to define the significant role of kinetic characteristics on the materials properties. The relations describing the thermodynamic and kinetics parameters are given in [Supplementary two](#). Moreover, the statistical description of the data space of the alloy attribute set is provided in [Table S2 supplementary two](#). After defining key attributes, it is necessary to normalize and condense broad range of parameters to a predefined domain. This procedure, namely min–max rescaling process, facilitates the learning practice in the neural network model [37]. Following the preliminary preparations, the learning process can presently be applied using CBNN model (detailed in section 3–2).

### 3.2. Correlation-based neural network (CBNN) approach

There are several accessible machine learning algorithms in WEKA library applied for GFA estimation of glassy alloys concerning second-generation features. The outcomes demonstrate the satisfactory performance of algorithms; however, it seems that there is still a long path to achieve ideal predictive models for design of novel MG alloys. The complex and interactive parameters with strong dependencies and correlations affecting the glass formation of liquid alloys. Hence, it is very critical to developing some predictive models being able to involve

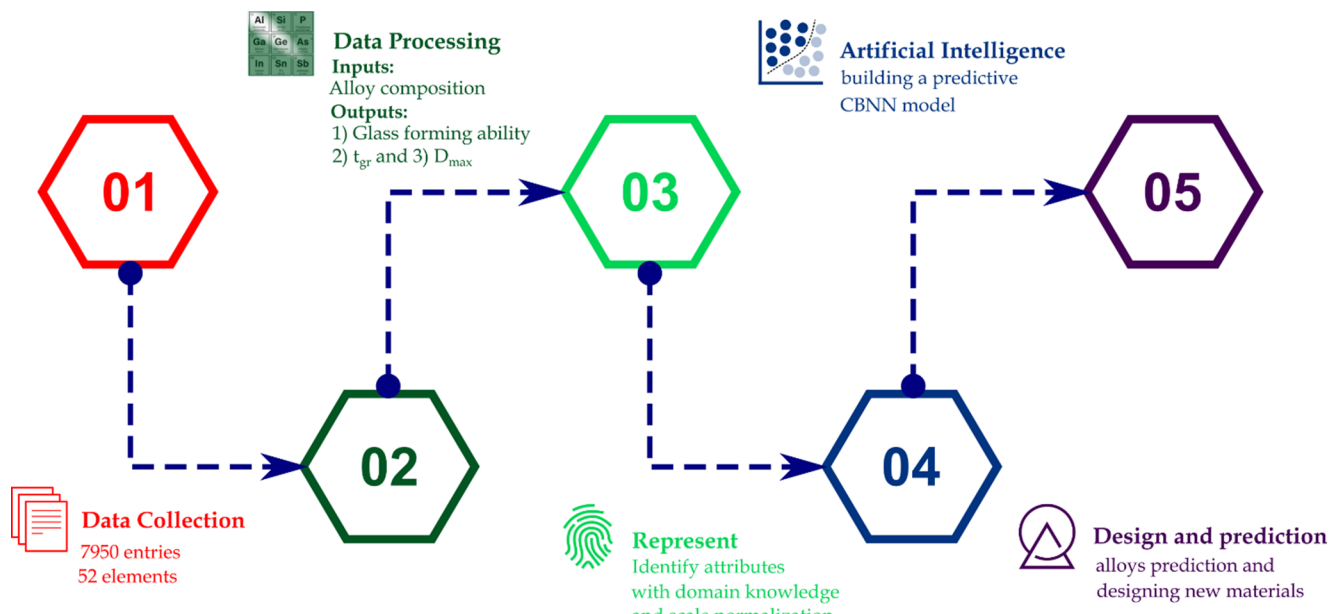


Fig. 1. Schematic of processing evolution for building the CBNN model.

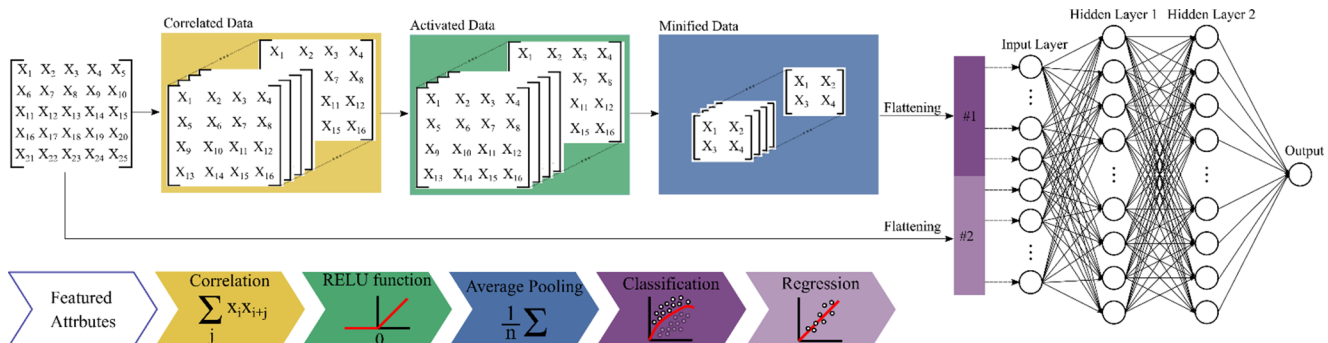


Fig. 2. Pictorial description of the CBNN structure employed in this study. Each dataset was correlated with 20 correlation  $2 \times 2$  matrices, the outputs were nonlinearly activated using ReLU function and then minified with average pooling. A total of 80 flattened features in addition to initial 25 scaled feature candidates were generated. 105 generated features were utilized for training 2-level fully connected neural network. Training process tried to obtain the weights of fully connected neural network and also find the 20 correlation  $2 \times 2$  matrices.

individual, mutual and multilateral characteristics of parameters for improvement of estimating process. To gain this goal, we develop a novel artificial intelligence algorithm, namely correlation-based neural network (CBNN), considering any inherent relevance of attributes. Attending the pictorial presentation of CBNN model (See Fig. 2), the algorithm tracks two unique route followed by a deep learning process with fully connected layers. The first route straightly transfers the data into the deep neural network, while the second route includes steps correlating input attributes using trained correlation matrices. This procedure enfolds both mutual and individual influence of essential attributes making the prediction model more reliable. In general, the data cross-correlation along with subsequent data activation and minification are performed before the deep learning process. To keep in touch with CBNN model, the steps are explained in Appendix A. Moreover, the composed code necessary for our CBNN model performance is given in *Supplementary three*.

### 3.3. Experimental procedure

In order to validate the CBNN model, it was required to produce some BMG alloys with certain chemical compositions, optimized GFA and critical thickness. At first, the master alloys with high purity elements (purity  $\geq 99.9\%$ ) were provided using vacuum arc re-melting for

four times under a Ti-gettered argon atmosphere and then cast by copper mold suction technique in the form of rods by Edmund Buhler compact arc melter MAM-1. The prepared specimens were cut and thereafter differential scanning calorimeter (DSC) analysis (STA6000 PerkinElmer) at the heating rate of 20 K/min was carried out to attain  $T_g$  and  $T_f$ . The X-ray diffraction (XRD) analysis (Rigaku Ultima IV) was also done to ensure the amorphousness of cast alloys.

## 4. Results and discussion

### 4.1. Examination of CBNN predictive model

The first objective in a predictive framework is to justify the model implemented for materials prognosis. Fig. 3a shows the receiver operating characteristic curve defining the predictive classification of casting capability in amorphous alloys. The result indicates that the CBNN model has an outstanding performance with the high precise true positive rate of 98% to discern BMGs from other classified alloys. The CBNN model also carefully distinguished the crystalline alloys and MG ribbons with accuracy of 96% and 95%, respectively, which implies the efficiency of the predictive model as an excellent classifier. The plots of CBNN-predicted values against the measured ones for  $T_{rg}$  and  $D_{max}$  are presented in Fig. 3b, c, respectively. For  $D_{max}$  evaluation, the dataset

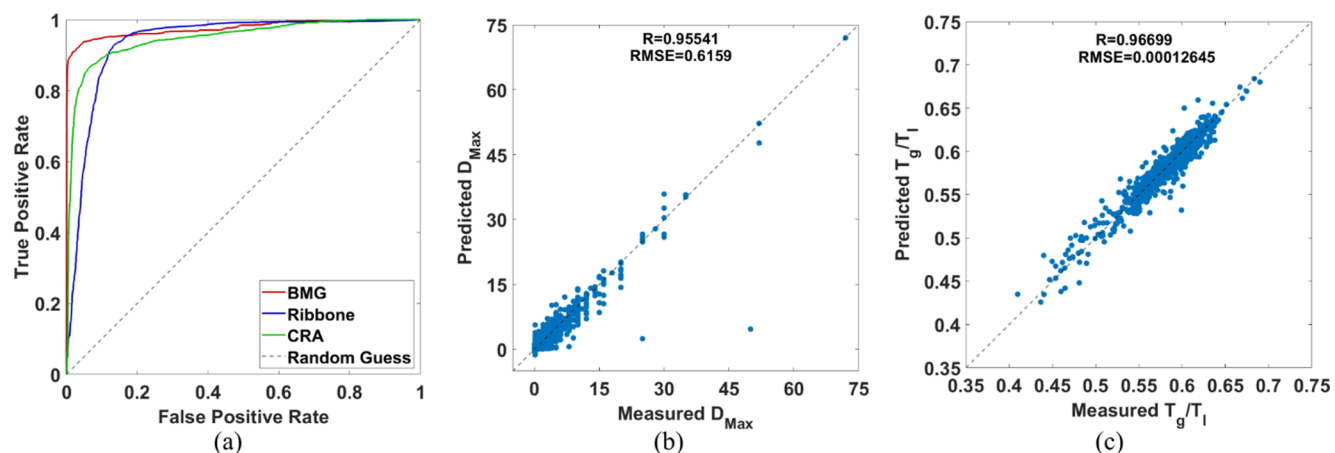


**Fig. 3.** a) Receiver operating characteristic curve showing the performance of classification model, and efficiency of regression model for b) critical thickness ( $D_{\max}$ ) and c) reduced glass transition ( $T_g$ ).

indeed includes the alloys with the reported maximum thickness. As observed, the root mean square error (RMSE) of 0.6159 mm and correlation coefficient ( $R$ ) of 0.95541 show that the CBNN model has a competent predictive performance. Nevertheless, there are just two outliers with chemical compositions of  $Zr_{41.2}Ti_{13.8}Cu_{12.5}Ni_{10}Be_{22.5}$  ( $D_{\max} = 50$  mm) and  $Y_{20}Sc_{36}Al_{24}Co_{20}$  ( $D_{\max} = 25$  mm), which were obviously separated from the main trend. This extreme underestimation may be due to the insufficient input data with similar alloy compositions or the mistakes made in the previous experimental works. Another interesting point is the exact prediction of  $Pd_{40}Cu_{30}Ni_{10}P_{20}$  BMG with 72 mm critical thickness, which was an Achilles' heel in the previous predictive model [31]. Our  $T_g$  validation test with  $R = 0.96699$  also has an evident converge data trend, which indicates the model proficiency for the GFA estimation of new MG alloys. This achievement, i.e. accurate prediction, is definitely resulted from the CBNN model providing correlative functions to support the attributes' dependency. Adapted to the convolutional neural network, the CBNN approach considers the attributes individually, mutually and multilaterally so that multiple correlative matrices are involved to process the inputs for the learning process and consequently develop a powerful adaptive prediction model for the novel materials recognition. Moreover, the CBNN approach includes a considerable variety of parameters for training process. While other thermodynamics or physical approaches are limited to few parameters or alloying compositions. For example, Kim et al [6] proposed their thermodynamics model based on the calculation of driving forces for crystalline phases under the undercooled liquid state. In contrast with other thermodynamics criteria [67]. They believed that the GFA may be inversely correlated to the nucleation kinetics in undercooled liquids and the driving force can be an acceptable concept for estimation of alloying composition. On the other side, another showed that  $\sigma$  parameter is a better criterion in comparison with  $T_g$  or  $\gamma$  to estimate the GFA for Ca-based BMGs [9]. It was also found that the critical cooling rate of a metallic liquid for glass formation strongly depends on the valence concentration of the liquid [10]. To wrestle this challenge, building a model based on artificial intelligence, containing several parameters with consideration of their mutual interactions, would be the basic solution. It should be noted that although, our model accurately predicts the GFA for various alloying compositions, it is unable to characterize the glass stability, which was considered in some other criteria [68].

#### 4.2. A case study

In recent years, Zr-Co-Al alloy system has been identified for producing possible BMGs with good GFA and large thickness [55,69–71]. Hence, it is suggested that the Zr-Co-Al system has potential for design

of new alloying compositions to fabricate promising glassy alloys with excellent glass formation and large critical diameters. For this purpose, we considered Zr-Co-Al-X quaternary alloys to assay our CBNN model. For this purpose, the W, Si, Ni elements were added into the Zr-Co-Al system as much as 5 at.% to unravel the role of the micro-alloying process on the GFA distribution of selected ternary alloy. The minor-added elements were picked out premeditatedly with different elemental classifications, i.e. metalloid, intermediate metallic and refractory, and a broad range of negative heat of mixing, presented in [Supplementary two](#). In order to evaluate the minor addition on the ternary system, it is very important to determine certain criteria for the data process and presentation. Hence, using CBNN classification model we detected the chemical compositions with glass forming possibility (GFP) of more than 50% in each alloying system. This detecting process includes all the chemical compositions in the Zr-Co-Al ternary system with the accuracy of 1 at.%. As given in [Fig. 4a](#), the GFP map of Zr-Co-Al ternary alloy shows that a remarkable set of alloying compositions (yellow color) has the opportunity less than 50% to create any glassy material. On the other side, two separated regions with acceptable GFP indicated that the ternary system may be able to form plentiful Zr-Co-based MGs in a wide range of alloying compositions; however, the amorphous Al-rich alloys also have chances in some extent. [Fig. 4b](#) illustrates the  $T_g$  distribution for the possible regions extracted from the GFP map of ternary Zr-Co-Al system. It is clear that the maximum  $T_g$  values are intensified in a high concentrated CoAl region with alloying composition range of  $Zr_{27-38}Co_{32-60}Al_{20-40}$ , which is due to the optimum electronegativity difference between Al and Co elements leading to the quasi-covalent bonds with strong liquid behavior [72]. In other words, the covalent bonds show strong interactions undertaking high atomic packing density with intensified short range ordering (SRO) structure. With all these descriptions, a region with high Zr concentration, i.e.  $40\% < Zr$  less than 70%, also shows a good glass forming ability in the ternary system and there are also some few compositions at the Zr line with excellent GFA indicating the casting capability of Zr-Al binary amorphous alloys, which is associated to the deep eutectic transitions. [Fig. 4c-e](#) illustrates the  $T_g$  distribution for the ternary system alloyed with 5 at.% W, Si and Ni, respectively. Regarding to the plots, one can see that the minor addition of elements expands the GFP area and averagely increases the  $T_g$  in the alloying system; however, the distribution of critical glass forming regions alters which is due to the individual effects of each added element. Although, the rise in heat of mixing and configurational entropy are the general reasons for GFP extension in the designed quaternary systems, it is required to study each system individually. According to the  $(ZrCoAl)_{95}W_5$  plot and compared to our basic ternary system, tungsten increases the GFP at high Al concentration and shifts the intensified  $T_g$  region (yellow color)

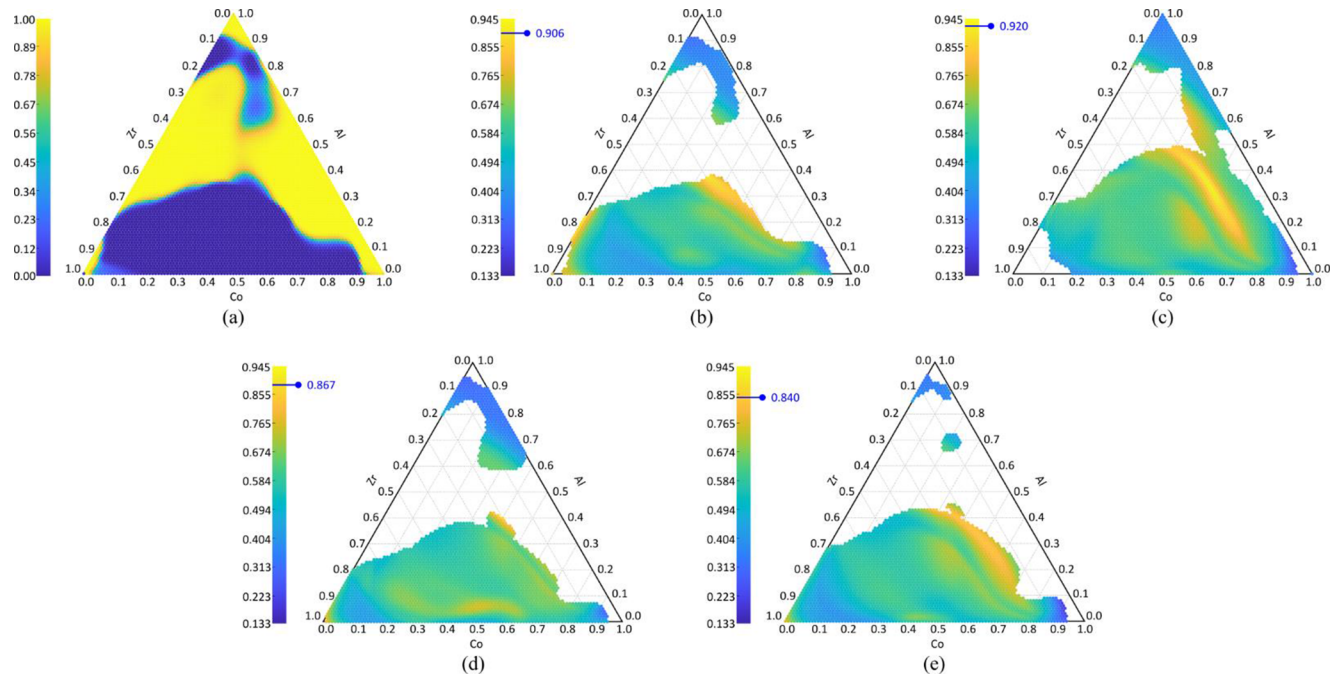


**Fig. 4.** a) ZrCoAl crystallization map, and  $T_{rg}$  distribution for b) ZrCoAl, c)  $(\text{ZrCoAl})_{95}\text{W}_5$ , d)  $(\text{ZrCoAl})_{95}\text{Si}_5$ , e)  $(\text{ZrCoAl})_{95}\text{Ni}_5$  systems.

to the higher Co content. It is also worth-mentioning that the mean  $T_{rg}$  in Zr-rich region significantly improves; however, there is no more chance for glass formation at compositions with more than 80 at% Zr. It is believed that tungsten with relatively large radius and high atomic weight not only enhances the viscosity but also reinforces the backbone in the amorphous structure leading to the higher atomic packing density [64]. This phenomenon especially appears in the GFP extension of Co- and Al-rich areas including sharper atomic mismatches. For  $(\text{ZrCoAl})_{95}\text{Si}_5$  plot, the GFP area moderately increases at Al- and Co-rich sites; however, the  $T_{rg}$  sharpness pales into insignificance. On the other side, the Zr-rich region shows a better GFA behavior than that observed in the Zr-Co-Al ternary system, given in Fig. 4b. It is suggested that small Si atoms may occupy interstitial sites among other constitutional spaces in the Zr-rich structure and form strong atomic bonding with their metallic neighbors leading to the liquid stabilization and SRO structure enhancement [72]. Probably the low atomic mismatch between Si, Co and Al prevents significant GFA improvement in Co- and Al-rich regions; however, the apparent solubility of Si into the mentioned regions makes a homogeneously alloying process leading to the broad GFP domain. In the  $(\text{ZrCoAl})_{95}\text{Ni}_5$  system, the sharp increase in total heat of mixing along with significant bonding interaction with Zr and Co atoms make the Zr- and Co-rich regions good glass formers. On the other side, the solubility lacking in the Al-rich system restricts the homogeneous alloying distribution and induces crystallization leading to the confined GFP region.

Beyond all the mentioned descriptions, it was discovered that there exists a strong relation between minor addition, the local structures and GFA in developed glassy alloys [72,73]. To deepen our study, we evaluate the types of possible atomic clusters created in the MG systems. Following Ref [5,31], there is an equation estimating the cluster radius in the alloying system:

$$R^X|_{x=i,j,k,s} = \frac{r_x Z_{x,\text{tot}}}{n_i Z_{xi} + r_j Z_{xj} + r_k Z_{xk} + r_s Z_{xs}}$$

In which  $R^X|_{x=i,j,k,s}$  is effective radius ratio in X-centred clusters,  $r_{i,j,k,s}$  is atomic radius of constituents,  $Z_{x,\text{tot}}$  is the number of neighboring atoms and  $Z_{i,x}$  defines the partial coordination number which is assumed in the range of 20 at.% for individual composition of each constitutional element in a cluster. The MGs are composed of various

types of clusters building the backbone of structure. These clusters appear when their effective radius ratio ( $R^X$ ) is close to the ideal radius ratio ( $r^*$ ) for the certain cluster; i.e.  $0.97 < \frac{R^X}{r^*} < 1.03$  [5]. Hence, in this work the possible ideally packed clusters with 9, 10, 12, 13, 15, 17 coordination numbers (CN) were identified to elaborate how the minor addition affects the short range structural ordering in the MG alloys. Since we will focus on the Zr-rich system in the following, a certain alloying composition, i.e.,  $(\text{Zr}_{65}\text{Co}_{20}\text{Al}_{10})_{95}\text{X}_5$ , at this region was considered for evaluation of cluster distribution. It is noted that the alloying composition was selected somehow to show better GFA with minor addition. Table 1 and Supplementary four gives the possible packed cluster types in selected BMG alloys. As a topological viewpoint, it can be concluded that the increase in types of clusters, including large or small ones, stabilizes the liquid and improves the GFA. However, it is very important that the increase in cluster types stays on a close CN. Hence, one can see that the Ni- and Si-centered clusters topologically seem to be more favored for the GFA enhancement. This result is confirmed by this hypothesis that the clusters with multiple equally likely arrangements in the liquid create a confused structure making the nucleation very difficult; however, the sharp variances may energetically induce crystallization [74]. Although, our mentioned calculations correctly interpret the GFA evolution in the certain alloy composition, the population of clusters or liquid-in type clusters are ignored, which suggests more investigations at this case in the future.

Again we turn our attention from an individual alloying composition to the in-group evaluation. The CBNN analysis indicated that the

**Table 1**  
Possible packed cluster types in BMG alloys.

Chemical composition	$T_{rg}$	CN = 9	CN = 10	CN = 13	CN = 15
$\text{Zr}_{65}\text{Co}_{20}\text{Al}_{15}$	0.501	[0, 0, 0, 0]	[0, 7, 7, 0]	[0, 0, 0, 0]	[12, 0, 0, 0]
$(\text{Zr}_{65}\text{Co}_{20}\text{Al}_{15})\text{W}_5$	0.556	[0, 0, 0, 0]	[0, 8, 3, 0]	[0, 0, 0, 3]	[26, 0, 0, 0]
$(\text{Zr}_{65}\text{Co}_{20}\text{Al}_{15})\text{Si}_5$	0.641	[0, 0, 0, 5]	[0, 7, 6, 0]	[0, 0, 0, 0]	[18, 0, 0, 0]
$(\text{Zr}_{65}\text{Co}_{20}\text{Al}_{15})\text{Ni}_5$	0.604	[0, 0, 0, 0]	[0, 9, 6, 9]	[0, 0, 0, 0]	[19, 0, 0, 0]

\*The numbers in bracket show the variety of cluster types with certain cores [Zr, Co, Al, X].

\*\*covalent radius ( $R_c$ ) was used to calculate the cluster numbers.

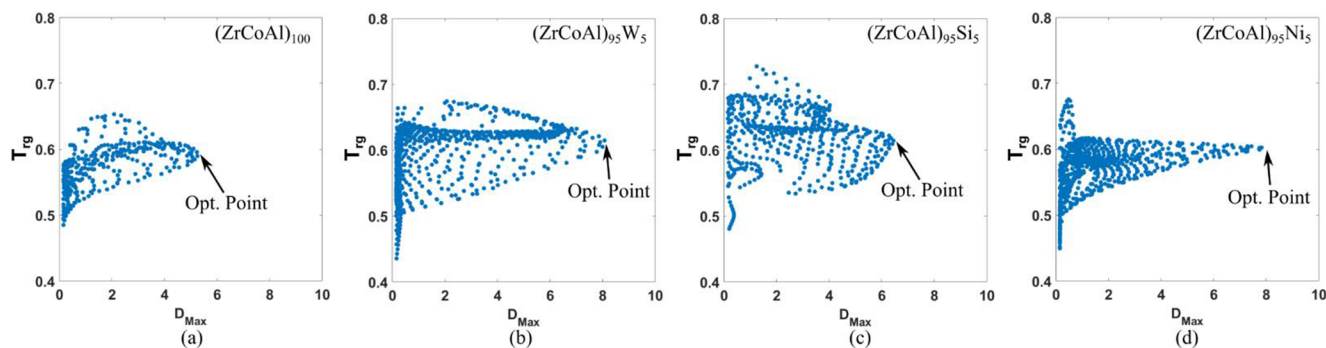


Fig. 5.  $T_g$  distribution as a function of  $D_{\max}$  for a) ZrCoAl, b)  $(\text{ZrCoAl})_{95}\text{W}_5$ , c)  $(\text{ZrCoAl})_{95}\text{Si}_5$ , d)  $(\text{ZrCoAl})_{95}\text{Ni}_5$  systems.

Table 2

BMGs with optimized  $T_{\text{rg}}$  and maximum  $D_{\max}$  in each alloying system.

Alloying compositions	BMG GFP (%)	$T_g$ (k)	$T_l$ (k)	$T_{\text{rg}}$	$D_{\max}$ (mm)
$\text{Zr}_{55}\text{Co}_{31}\text{Al}_{14}$	98.9	743	1260	0.589	5.26
$(\text{Zr}_{61}\text{Co}_{14}\text{Al}_{25})_{95}\text{W}_5$	100	804	1308	0.615	8.08
$(\text{Zr}_{59}\text{Co}_{21}\text{Al}_{20})_{95}\text{Si}_5$	99.8	739	1203	0.614	6.45
$(\text{Zr}_{64}\text{Co}_{18}\text{Al}_{18})_{95}\text{Ni}_5$	99.9	715	1188	0.602	7.83

$T_{\text{rg}}$  improvement in Al- and Co-rich compositions, due to the minor addition, does not accompany with significant  $D_{\max}$  increasing, while the Zr-rich region includes both GFA and  $D_{\max}$  alteration. Thereupon, to study the GFA evolution, the  $T_{\text{rg}}\text{-}D_{\max}$  distribution maps of the alloying systems with Zr greater than 50 at.% and  $D_{\max}$  greater than 0.15 mm are represented in Fig. 5. The results indicate that trend of plots is in a way to reach an optimized  $T_{\text{rg}}$  for the maximum critical thickness, which is similar to that happened in ref. [31]. Again it is very important to be attended that our evaluation is not limited to the specific chemical composition and comprises a broad range of MG alloys with Zr greater than 50 at.%. In the ternary system, the CBNN model predicts that an amorphous alloy ( $\text{Zr}_{55}\text{Co}_{31}\text{Al}_{14}$ ) with 5.26 mm thickness can be produced (see Table 2). According to Supplementary five, the maximum thicknesses achieved when the Co/Al ratio is more than 1. With W addition, the variety of BMG alloys with different thicknesses and  $T_{\text{rg}}$  increases and the  $D_{\max}$  exceeds more than 8 mm. It is also revealed that the suitable Co/Al ratio for attaining high  $T_{\text{rg}}$  and  $D_{\max}$  is a little less than 1. At the first glance, it may be concluded that the Al-W bonding formation is favored in the structure; however, the cluster configurations suggest no strong Al-W interactions. This result emphasizes that the minor addition necessarily does not establish an interactive relation with rich elements to produce specific clusters and it may act as an elemental homogenizer or leveler for the cluster types, which is discussed before. Similar to the tungsten addition, The Si atoms extend the  $T_{\text{rg}}\text{-}D_{\max}$  distribution in the alloying system; however, the significant lower  $T_g$  and  $T_l$  values show that the metalloid atoms tend to decrease the melting temperature of predicted alloys. Achieving large  $D_{\max}$ , it is required to move to a balanced Al/Co ratio. Unlike mentioned cases, the Ni addition tend to converge  $T_{\text{rg}}\text{-}D_{\max}$  plot resulting the optimized  $T_{\text{rg}}$  of 0.602 and  $D_{\max}$  of 7.83 mm. The converged temperature characteristics along with thick BMG formation with more than 60 at.% is derived from large negative heat of mixing of Zr-Ni bonds, deep eutectic events and diverse 10-CN clusters generated in the structure. In the next step, in order to justify our model we considered a 3-mm-predicted alloy composition with the maximum  $T_{\text{rg}}$  from each system for the experimental casting process. For this purpose, each alloying composition was cast in the form of rods with 2-, 3- and 4-mm diameters. The DSC and XRD curves for amorphous alloying compositions are presented in Fig. 6. As given in Table 3, the W-contained alloy has the experimental  $D_{\max}$  of 2 mm, which is lower than the predicted condition. The other predicted alloying compositions in Table 3 were affirmed by experimental casting process in the form of 3-mm amorphous

rods. In all cases, the crystalline phases appear in the 4-mm cast rods (not given here) indicating the acceptable thickness prediction of our CBNN model. Moreover, the  $T_g$  and  $T_l$  values, obtained from DSC measurements, demonstrate that the experimental and prediction results have a meaningful closeness.

After minor addition analysis, a complete quaternary system was selected for further evaluations. Some studies reported that the added element with positive heat of mixing enhances the GFA in an alloying system; however, this event is restricted to the microalloying process [59,75]. In other words, the excessive addition of element with positive heat of mixing may lead to the nanocrystallization or severe phase separation in the glassy structure [76]. On the other side, when all the constituents comprise the negative heat of mixing, it is possible to explore alloying systems with good GFA and high entropic behavior [77]. Evaluating several elements with negative heat of mixing in ZrCoAl system, our CBNN model revealed that the Ni element as a fourth constituent in ZrCoAl alloying system is able to extend the GFP area in a wide range of chemical composition and produce monolithic glassy structure. Fig. 7 illustrates layered-by-layered GFP diagram of  $\text{ZrCoAlNi}$  quaternary alloy with the Ni variations. Enhancing the total negative heat of mixing, the Ni addition leads to the GFP extension in the system. This improvement continues up to 40 at.% Ni addition and comes to the detriment of glass forming at Al-rich regions. With higher Ni concentrations, the GFP area significantly declines and is limited to the NiZr-rich alloys which may be due to the strong interactive of Zr-Ni bonds. The intensified effect of Ni at the range of 20–40 at.% also suggests that the designed system has potential for the engineering of high entropy BMGs. For this purpose, it is necessary to add one or more elements to the system for producing a multiple major-element alloy. However, the added elements should activate the Al-rich part of system at the range of 20–30 at.% as the glass formers. Based on the analyses in this work, W and Si atoms are potential elements generating the Al-rich GFP area, improving the atomic size mismatches and having a positive effect on mixing entropy and heat of mixing in the engineered high-entropy BMG. In a summary, it is concluded that the CBNN framework is able to provide a path for engineering of novel BMG compositions. Moreover, the inherent characteristics of CBNN approach, i.e. deep correlating of attributes, encourage researchers to develop innovative predictive models for other materials classifications.

## 5. Conclusions

This work offers a developed correlation-based neural network (CBNN) approach for designing new MG alloys with prediction of casting ability, maximum thickness and reduced glass transition temperature. The correlative learning of parameters in the CBNN model along with a huge dataset composed of 7950 alloying systems leads to the building of an efficient predictive tool, validated by the experimental cast process. Adopting this model, we evaluated the minor addition of W, Si and Ni on the ZrCoAl ternary system and identified the influential mechanism of each element on the glass forming possibility.

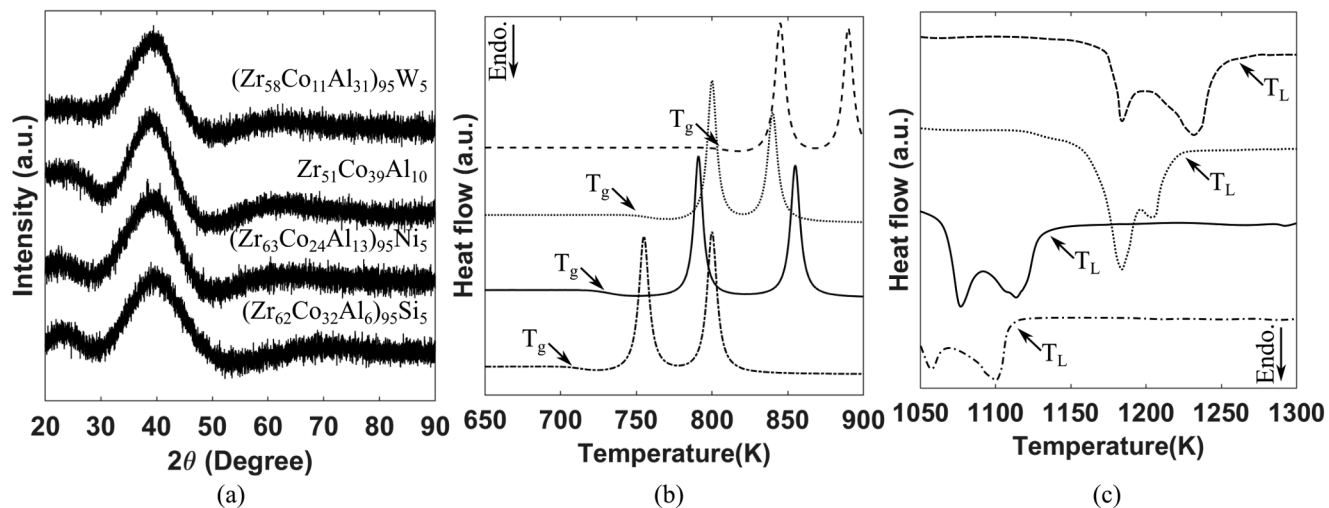


Fig. 6. a) XRD patterns and b) DSC curves for selected samples with amorphous structure.

Table 3

Experimental and prediction data for BMG compositions with  $\sim 3$  mm  $D_{\max}$ .

Alloying compositions	Pred. $T_g$	Pred. $T_l$	Pred. $T_{rg}$	Pred. $D_{\max}$	Exp. $T_g$	Exp. $T_l$	Exp. $T_{rg}$	Exp. $D_{\max}$
$\text{Zr}_{51}\text{Co}_{39}\text{Al}_{10}$	748	1195	0.626	3.07	759	1221	0.621	3
$(\text{Zr}_{58}\text{Co}_{11}\text{Al}_{31})_{95}\text{W}_5$	828	1242	0.666	3.02	809	1279	0.632	2
$(\text{Zr}_{62}\text{Co}_{32}\text{Al}_6)_{95}\text{Si}_5$	727	1086	0.675	3.09	714	1112	0.642	3
$(\text{Zr}_{63}\text{Co}_{24}\text{Al}_{13})_{95}\text{Ni}_5$	711	1160	0.613	3.08	732	1123	0.651	3

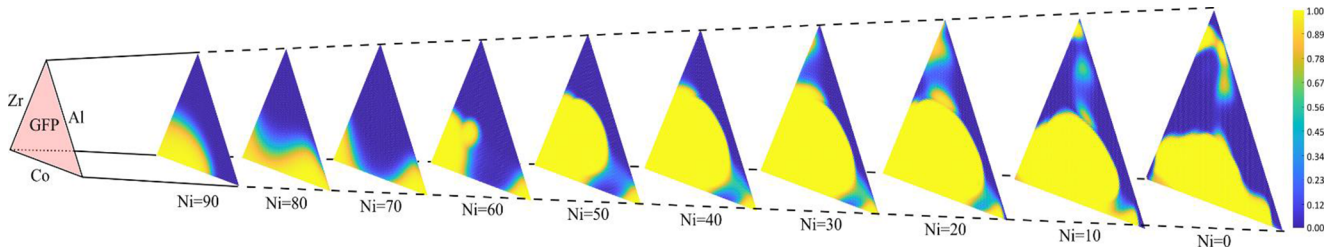


Fig. 7. GFP map for  $\text{ZrCoAlNi}$  quaternary system.

Moreover, our model predicted the  $\text{ZrCoAlNi}$  alloying system with high glass forming possibility at the wide range of chemical compositions. Finally, it is suggested that this framework will be able to detect novel BMGs in the quaternary systems and facilitate their engineering process for potential applications.

#### Declaration of Competing Interest

The authors declare that they have no known competing financial interests or personal relationships that could have appeared to influence the work reported in this paper.

#### Appendix A:

There are several Machine Learning (ML) algorithms, including linear ML algorithms, nonlinear ML algorithms and ensemble ML algorithms commonly used in earlier literature [37,78]. In this research, we are proposing a new artificial intelligence algorithm called the correlation based neural network (CBNN), capturing correlations among the feature candidates. The CBNN model steps are follow as:

#### Correlating layer

Cross-correlation of the attributes is the core component of CBNN and uses several correlating matrices to extract the salient correlated features of attributes. The first layer takes the input scaled attributes and then fulfills cross-correlation of the attributes with multiple correlative matrices eventually ensuing manifold correlated datasets. As to the number of matrices, each dataset specifies a particular feature. The correlating layer

#### Acknowledgment

This work was supported by the Iran National Science Foundation (INSF) (Grants No. 98019920).

#### Data availability

The raw/processed data required to reproduce these findings cannot be shared at this time as the data also forms part of an ongoing study.

applied in this stage is mathematically represented as:

$$\mathbf{y}[i, j] = \sum_{a=0}^{c-1} \sum_{b=0}^{r-1} \mathbf{w}[a, b] \mathbf{x}[i + a, j + b] \quad (A1)$$

In which  $\mathbf{x}$  and  $\mathbf{w}$  define the input scaled attribute matrix and the correlating matrix, respectively. A discrete output of the correlating layer is introduced by  $\mathbf{y}$  [i,], while r and c are the row and column of correlating matrix.

#### Activating layer

To improve our algorithm as predictive model, we progressed the output  $\mathbf{y}$  from Eq. (1) in a nonlinear activation function. For this purpose, Rectified Linear Unit (ReLU) activation function was applied:

$$\text{ReLU}(x) = \begin{cases} 0 & \text{if } x < 0 \\ x & \text{if } x \geq 0 \end{cases} \quad (2)$$

In this regard, the mentioned function takes the input-output nonlinear complex functional mappings. In our work, all the correlated datasets were involved in the activation function. As a consequence, the notable correlated features are figured out.

#### Pooling layer

In order to minimize the calculations and manipulations a down sampling is used. This down sampling is called pooling layer and the outcomes are comprising all the salient data over each dataset. Hand in hand of lowering the computational operations, average pooling is the most effective pooling method and mathematically described as

$$\text{Pool}(x, y) = \sum_{j=0}^{q-1} \sum_{i=0}^{q-1} \frac{I(q \times x + i, q \times y + j)}{q^2} \quad (3)$$

where  $(x, y)$  defines the output of the correlated data after average pooling and  $q$  determines the coarsening length in average pooling.

#### Fully connected artificial neural network

The correlated minimized data, called data group #1, along with the feature attributes, called data group #2, are merged to a vector called data vector. Then, the data vector are inserted into a multilayer conventional artificial neural network. Each layer in the conventional artificial neural network analyses the data of its previous layer through several neurons which may formulated as

$$\gamma_i^\ell = f \left( \sum_{j=1}^{N_{\ell-1}} \omega_{ij}^l \gamma_j^{\ell-1} + b_i \right) i = 1, \dots, N_\ell \quad (4)$$

where  $N_l$  and  $N_{l-1}$  are the number of the  $l^{th}$  and  $(l-1)^{th}$  layers, respectively.  $\gamma_i^\ell$  is the output of the  $i^{th}$  neuron in the  $l^{th}$  layer with  $\omega_{ij}^l$  as the weight factors relating the inputs to a certain output and  $b_i$  as the bias value.  $f$  is the ReLU activation function described in (2). CANN is a generalized function estimator that will be able to adjust the weights and biases terms in order to forecast any input/output interaction with adequate accuracy. Such parameters are changed during the training process, typically by applying a back-propagation algorithm.

#### Appendix B. Supplementary data

Supplementary data to this article can be found online at <https://doi.org/10.1016/j.commatsci.2020.110025>.

#### References

- [1] Y. Sun, A. Concstell, A.L. Greer, Thermomechanical processing of metallic glasses: extending the range of the glassy state, *Nat. Rev. Mater.* 1 (2016) 16039, <https://doi.org/10.1038/natrevmats.2016.39>.
- [2] W.H. Wang, Dynamic relaxations and relaxation-property relationships in metallic glasses, *Prog. Mater Sci.* 106 (2019) 100561, , <https://doi.org/10.1016/j.pmatsci.2019.03.006>.
- [3] M. Samavatian, R. Gholamipour, A.A. Amadeh, S. Mirdamadi, Role of tensile elastostatic loading on atomic structure and mechanical properties of Zr55Cu30Ni5Al10 bulk metallic glass, *Mater. Sci. Eng., A* 753 (2019) 218–223, <https://doi.org/10.1016/j.msea.2019.03.058>.
- [4] J. Schroers, Processing of bulk metallic glass, *Adv. Mater.* 22 (2010) 1566–1597, <https://doi.org/10.1002/adma.200902776>.
- [5] K.J. Laws, D.B. Miracle, M. Ferry, A predictive structural model for bulk metallic glasses, *Nat. Commun.* 6 (2015) 8123, <https://doi.org/10.1038/ncomms9123>.
- [6] D. Kim, B.-J. Lee, N.J. Kim, Prediction of composition dependency of glass forming ability of Mg–Cu–Y alloys by thermodynamic approach, *Scr. Mater.* 52 (2005) 969–972, <https://doi.org/10.1016/j.scriptamat.2005.01.038>.
- [7] N. Neuber, O. Gross, M. Eisenbart, A. Heiss, U.E. Klotz, J.P. Best, M.N. Polyakov, J. Michler, R. Busch, I. Gallino, The role of Ga addition on the thermodynamics, kinetics, and tarnishing properties of the Au-Ag-Pd-Cu-Si bulk metallic glass forming system, *Acta Mater.* 165 (2019) 315–326, <https://doi.org/10.1016/j.actamat.2018.11.052>.
- [8] A. Radoń, P. Włodarczyk, Ł. Hawelek, M. Kadziolka-Gawel, P. Gębara, R. Nowosielski, R. Babilas, Thermodynamic approach for determining chemical composition of Fe-Co based amorphous alloys with high thermal stability and glass forming ability, *J. Alloy. Compd.* 763 (2018) 141–152, <https://doi.org/10.1016/j.jallcom.2018.05.242>.
- [9] E.S. Park, D.H. Kim, Effect of atomic configuration and liquid stability on the glass-forming ability of Ca-based metallic glasses, *Appl. Phys. Lett.* 86 (2005) 201912, , <https://doi.org/10.1063/1.1931832>.
- [10] Q. Jiang, B.Q. Chi, J.C. Li, A valence electron concentration criterion for glass-formation ability of metallic liquids, *Appl. Phys. Lett.* 82 (2003) 2984–2986, <https://doi.org/10.1063/1.1571984>.
- [11] Y.-C. Hu, J. Schroers, M.D. Shattuck, C.S. O'Hern, Tuning the glass-forming ability of metallic glasses through energetic frustration, *Phys. Rev. Mater.* 3 (2019) 85602, <https://doi.org/10.1103/PhysRevMaterials.3.085602>.
- [12] S. Bera, S. Paul, P. Ramasamy, D. Mandal, M. Das, A. Lassnig, O. Renk, M. Calin, J. Eckert, Synthesis of new glassy Mg–Ca–Zn alloys with exceptionally low Young's Modulus: exploring near eutectic compositions, *Scr. Mater.* 173 (2019) 139–143, <https://doi.org/10.1016/j.scriptamat.2019.08.009>.
- [13] J. Schmidt, M.R.G. Marques, S. Botti, M.A.L. Marques, Recent advances and applications of machine learning in solid-state materials science, *npj Comput. Mater.* 5 (2019) 83, <https://doi.org/10.1038/s41524-019-0221-0>.
- [14] M.A.N. Dewapriya, R.K.N.D. Rajapakse, W.P.S. Dias, Characterizing fracture stress of defective graphene samples using shallow and deep artificial neural networks,

- Carbon N. Y. 163 (2020) 425–440, <https://doi.org/10.1016/j.carbon.2020.03.038>.
- [15] A. Karakoc, Ö. Keleş, A predictive failure framework for brittle porous materials via machine learning and geometric matching methods, *J. Mater. Sci.* 55 (2020) 4734–4747, <https://doi.org/10.1007/s10853-019-04339-1>.
- [16] X. Liu, C.E. Athanasiou, N.P. Padture, B.W. Sheldon, H. Gao, A machine learning approach to fracture mechanics problems, *Acta Mater.* 190 (2020) 105–112, <https://doi.org/10.1016/j.actamat.2020.03.016>.
- [17] H. Zong, G. Pilania, X. Ding, G.J. Ackland, T. Lookman, Developing an interatomic potential for martensitic phase transformations in zirconium by machine learning, *npj Comput. Mater.* 4 (2018) 48, <https://doi.org/10.1038/s41524-018-0103-x>.
- [18] J. Timoshenko, A. Anspoks, A. Cintins, A. Kuzmin, J. Purans, A.I. Frenkel, Neural network approach for characterizing structural transformations by X-ray absorption fine structure spectroscopy, *Phys. Rev. Lett.* 120 (2018) 225502, , <https://doi.org/10.1103/PhysRevLett.120.225502>.
- [19] X. Huang, H. Wang, W. Xue, S. Xiang, H. Huang, L. Meng, G. Ma, A. Ullah, G. Zhang, Study on time-temperature-transformation diagrams of stainless steel using machine-learning approach, *Comput. Mater. Sci.* 171 (2020) 109282, , <https://doi.org/10.1016/j.commatsci.2019.109282>.
- [20] R. Kondo, S. Yamakawa, Y. Masuoka, S. Tajima, R. Asahi, Microstructure recognition using convolutional neural networks for prediction of ionic conductivity in ceramics, *Acta Mater.* 141 (2017) 29–38, <https://doi.org/10.1016/j.actamat.2017.09.004>.
- [21] N. Lubbers, T. Lookman, K. Barros, Inferring low-dimensional microstructure representations using convolutional neural networks, *Phys. Rev. E* 96 (2017) 52111, <https://doi.org/10.1103/PhysRevE.96.052111>.
- [22] A. Baskaran, G. Kane, K. Biggs, R. Hull, D. Lewis, Adaptive characterization of microstructure dataset using a two stage machine learning approach, *Comput. Mater. Sci.* 177 (2020) 109593, , <https://doi.org/10.1016/j.commatsci.2020.109593>.
- [23] S.K. Dewangan, S. Samal, V. Kumar, Microstructure exploration and an artificial neural network approach for hardness prediction in AlCrFeMnNiWx High-Entropy Alloys, *J. Alloy. Compd.* 823 (2020) 153766, , <https://doi.org/10.1016/j.jallcom.2020.153766>.
- [24] Z. Yang, Y.C. Yabansu, D. Jha, W. Liao, A.N. Choudhary, S.R. Kalidindi, A. Agrawal, Establishing structure-property localization linkages for elastic deformation of three-dimensional high contrast composites using deep learning approaches, *Acta Mater.* 166 (2019) 335–345, <https://doi.org/10.1016/j.actamat.2018.12.045>.
- [25] Z. Zhou, Y. Zhou, Q. He, Z. Ding, F. Li, Y. Yang, Machine learning guided appraisal and exploration of phase design for high entropy alloys, *npj Comput. Mater.* 5 (2019) 128, <https://doi.org/10.1038/s41524-019-0265-1>.
- [26] T.L.P. Galvão, G. Novell-Leruth, A. Kuznetsova, J. Tedim, J.R.B. Gomes, Elucidating structure-property relationships in aluminum alloy corrosion inhibitors by machine learning, *J. Phys. Chem. C* 124 (2020) 5624–5635, <https://doi.org/10.1021/acs.jpcc.9b09538>.
- [27] A. Majid, S.B. Ahsan, N. ul H. Tariq, Modeling glass-forming ability of bulk metallic glasses using computational intelligent techniques, *Appl. Soft Comput.* 28 (2015) 569–578.
- [28] M.K. Tripathi, P.P. Chattopadhyay, S. Ganguly, Multivariate analysis and classification of bulk metallic glasses using principal component analysis, *Comput. Mater. Sci.* 107 (2015) 79–87, <https://doi.org/10.1016/j.commatsci.2015.05.010>.
- [29] M.K. Tripathi, P.P. Chattopadhyay, S. Ganguly, A predictable glass forming ability expression by statistical learning and evolutionary intelligence, *Intermetallics* 90 (2017) 9–15, <https://doi.org/10.1016/j.intermet.2017.06.008>.
- [30] Y.T. Sun, H.Y. Bai, M.Z. Li, W.H. Wang, Machine learning approach for prediction and understanding of glass-forming ability, *J. Phys. Chem. Lett.* 8 (2017) 3434–3439, <https://doi.org/10.1021/acs.jpcllett.7b01046>.
- [31] L. Ward, S.C. O’Keeffe, J. Stevick, G.R. Jelbert, M. Aykolt, C. Wolverton, A machine learning approach for engineering bulk metallic glass alloys, *Acta Mater.* 159 (2018) 102–111, <https://doi.org/10.1016/j.actamat.2018.08.002>.
- [32] F. Ren, L. Ward, T. Williams, K.J. Laws, C. Wolverton, J. Hattrick-Simpers, A. Mehta, Accelerated discovery of metallic glasses through iteration of machine learning and high-throughput experiments, *Sci. Adv.* 4 (2018) eaau1566, <https://doi.org/10.1126/sciadv.aau1566>.
- [33] A. Cai, X. Xiong, Y. Liu, W. An, J. Tan, Y. Luo, Artificial neural network modeling for undercooled liquid region of glass forming alloys, *Comput. Mater. Sci.* 48 (2010) 109–114, <https://doi.org/10.1016/j.commatsci.2009.12.012>.
- [34] A.H. Cai, Y. Liu, W.K. An, G.J. Zhou, Y. Luo, T.L. Li, X.S. Li, X.F. Tan, Prediction of critical cooling rate for glass forming alloys by artificial neural network, *Mater. Des.* 52 (2013) 671–676, <https://doi.org/10.1016/j.matedes.2013.06.012>.
- [35] A. Cai, X. Xiong, Y. Liu, W. An, G. Zhou, Y. Luo, T. Li, X. Li, X. Tan, Compositional optimization of glass forming alloys based on critical dimension by using artificial neural network, *Trans. Nonferrous Met. Soc. China* 24 (2014) 1458–1466, [https://doi.org/10.1016/S1003-6326\(14\)63213-1](https://doi.org/10.1016/S1003-6326(14)63213-1).
- [36] J. Xiong, T.-Y. Zhang, S.-Q. Shi, Machine learning prediction of elastic properties and glass-forming ability of bulk metallic glasses, *MRS Commun.* 9 (2019) 576–585, <https://doi.org/10.1557/mrc.2019.44>.
- [37] J. Xiong, S.-Q. Shi, T.-Y. Zhang, A machine-learning approach to predicting and understanding the properties of amorphous metallic alloys, *Mater. Des.* 187 (2020) 108378, , <https://doi.org/10.1016/j.matedes.2019.108378>.
- [38] X. Liu, F. Li, Y. Yang, “Softness” as the structural origin of plasticity in disordered solids: a quantitative insight from machine learning, *Sci. China Mater.* 62 (2019) 154–160, <https://doi.org/10.1007/s40843-018-9316-2>.
- [39] A. Dasgupta, S.R. Broderick, C. Mack, B.U. Kota, R. Subramanian, S. Setlur, V. Govindaraju, K. Rajan, Probabilistic assessment of glass forming ability rules for metallic glasses aided by automated analysis of phase diagrams, *Sci. Rep.* 9 (2019) 357, <https://doi.org/10.1038/s41598-018-36224-3>.
- [40] Q. Wang, A. Jain, A transferable machine-learning framework linking interstice distribution and plastic heterogeneity in metallic glasses, *Nat. Commun.* 10 (2019) 5537, <https://doi.org/10.1038/s41467-019-13511-9>.
- [41] Y. Kawazoe, J.-Z. Yu, A.-P. Tsai, T. Masumoto, *Nonequilibrium Phase Diagrams of Ternary Amorphous Alloys*, first ed., Springer-Verlag, Berlin Heidelberg, 1997.
- [42] L. Ward, <https://citrination.com/datasets/156839>, n.d.
- [43] A.A. Deshmukh, A.A. Khond, J.G. Bhatt, U.A. Palankundwar, Understanding the role of Er on glass-forming ability parameters and critical cooling rate in Fe-based multicomponent bulk metallic glasses, *J. Alloy. Compd.* 819 (2020) 152938, , <https://doi.org/10.1016/j.jallcom.2019.152938>.
- [44] B. Li, W.C. Sun, H.N. Qi, J.W. Lv, F.L. Wang, M.Z. Ma, X.Y. Zhang, Effects of Ag substitution for Fe on glass-forming ability, crystallization kinetics, and mechanical properties of Ni-free Zr–Cu–Al–Fe bulk metallic glasses, *J. Alloy. Compd.* 827 (2020) 154385, , <https://doi.org/10.1016/j.jallcom.2020.154385>.
- [45] H. Jia, X. Xie, L. Zhao, J. Wang, Y. Gao, K.A. Dahmen, W. Li, P.K. Liaw, C. Ma, Effects of similar-element-substitution on the glass-forming ability and mechanical behaviors of Ti–Cu–Zr–Pd bulk metallic glasses, *J. Mater. Res. Technol.* 7 (2018) 261–269, <https://doi.org/10.1016/j.jmrt.2017.08.009>.
- [46] F. Hu, C. Yuan, Q. Luo, W. Yang, B. Shen, Effects of heavy rare-earth addition on glass-forming ability, thermal, magnetic, and mechanical properties of Fe–RE–B–Nb (RE = Dy, Ho, Er or Tm) bulk metallic glass, *J. Non. Cryst. Solids.* 525 (2019) 119681, , <https://doi.org/10.1016/j.jnoncrysol.2019.119681>.
- [47] F. Hu, Q. Luo, B. Shen, Thermal, magnetic and magnetocaloric properties of FeErNbB metallic glasses with high glass-forming ability, *J. Non. Cryst. Solids.* 512 (2019) 184–188, <https://doi.org/10.1016/j.jnoncrysol.2019.03.005>.
- [48] S. Hasani, P. Rezaei-Shahreza, A. Seifoddini, M. Hakimi, Enhanced glass forming ability, mechanical, and magnetic properties of Fe41Co7Cr15Mo14Y2C15B6 bulk metallic glass with minor addition of Cu, *J. Non. Cryst. Solids.* 497 (2018) 40–47, <https://doi.org/10.1016/j.jnoncrysol.2018.05.021>.
- [49] J.-L. Gu, Y. Shao, K.-F. Yao, The novel Ti-based metallic glass with excellent glass forming ability and an elastic constant dependent glass forming criterion, *Materialia* 8 (2019) 100433, , <https://doi.org/10.1016/j.mtla.2019.100433>.
- [50] J. Ge, H. He, J. Zhou, C. Lu, W. Dong, S. Liu, S. Lan, Z. Wu, A. Wang, L. Wang, C. Yu, B. Shen, X. Wang, In-situ scattering study of a liquid–liquid phase transition in Fe–B–Nb–Y supercooled liquids and its correlation with glass-forming ability, *J. Alloy. Compd.* 787 (2019) 831–839, <https://doi.org/10.1016/j.jallcom.2019.02.114>.
- [51] J. Zhu, C. Wang, J. Han, S. Yang, G. Xie, H. Jiang, Y. Chen, X. Liu, Formation of Zr-based bulk metallic glass with large amount of yttrium addition, *Intermetallics* 92 (2018) 55–61, <https://doi.org/10.1016/j.intermet.2017.08.018>.
- [52] G. Yang, J. Lian, R. Wang, N. Wu, Similar atom substitution effect on the glass forming ability in (LaCe)Al–(NiCo) bulk metallic glasses using electron structure guiding, *J. Alloy. Compd.* 786 (2019) 250–256, <https://doi.org/10.1016/j.jallcom.2019.01.339>.
- [53] Y.J. Yang, B.Y. Cheng, J.W. Lv, B. Li, M.Z. Ma, X.Y. Zhang, G. Li, R.P. Liu, Effect of Ag substitution for Ti on glass-forming ability, thermal stability and mechanical properties of Zr-based bulk metallic glasses, *Mater. Sci. Eng., A* 746 (2019) 229–238, <https://doi.org/10.1016/j.msea.2018.12.123>.
- [54] T. Wada, J. Jiang, K. Kubota, H. Kato, A. Takeuchi, Septenary Zr–Hf–Ti–Al–Co–Ni–Cu high-entropy bulk metallic glasses with centimeter-scale glass-forming ability, *Materialia* 7 (2019) 100372, , <https://doi.org/10.1016/j.mtla.2019.100372>.
- [55] Q. Dong, Y.J. Pan, J. Tan, X.M. Qin, C.J. Li, P. Gao, Z.X. Feng, M. Calin, J. Eckert, A comparative study of glass-forming ability, crystallization kinetics and mechanical properties of Zr55Co25Al20 and Zr52Co25Al23 bulk metallic glasses, *J. Alloy. Compd.* 785 (2019) 422–428, <https://doi.org/10.1016/j.jallcom.2019.01.180>.
- [56] L. Xue, J. Li, W. Yang, C. Yuan, B. Shen, Effect of Fe substitution on magnetocaloric effects and glass-forming ability in Gd-based metallic glasses, *Intermetallics* 93 (2018) 67–71, <https://doi.org/10.1016/j.intermet.2017.11.007>.
- [57] X. Song, X. Liu, Y. Yang, S. Feng, Y. Lu, J. Kong, Glass forming ability and a novel method for evaluating the thermoplastic formability of ZrxTi65-xBe27.5Cu7.5 alloys, *Intermetallics* 114 (2019) 106600.
- [58] D. Cao, Y. Wu, X.J. Liu, H. Wang, X.Z. Wang, Z.P. Lu, Enhancement of glass-forming ability and plasticity via alloying the elements having positive heat of mixing with Cu in Cu48Zr48Al4 bulk metallic glass, *J. Alloy. Compd.* 777 (2019) 382–391, <https://doi.org/10.1016/j.jallcom.2018.10.396>.
- [59] G. Cao, K. Liu, G. Liu, H. Zong, H. Bala, B. Zhang, Improving the glass-forming ability and the plasticity of Zr–Cu–Al bulk metallic glass by addition of Nb, *J. Non. Cryst. Solids.* 513 (2019) 105–110, <https://doi.org/10.1016/j.jnoncrysol.2019.03.009>.
- [60] M. Malekan, R. Rashidi, S.G. Shabestari, Mechanical properties and crystallization kinetics of Er-containing Cu–Zr–Al bulk metallic glasses with excellent glass forming ability, *Vacuum* 174 (2020) 109223, , <https://doi.org/10.1016/j.vacuum.2020.109223>.
- [61] R. Deng, Z. Long, L. Peng, D. Kuang, B. Ren, A new mathematical expression for the relation between characteristic temperature and glass-forming ability of metallic glasses, *J. Non. Cryst. Solids.* 533 (2020) 119829, , <https://doi.org/10.1016/j.jnoncrysol.2019.11.9829>.
- [62] S. Saini, A.P. Srivastava, S. Neogy, The effect of Ag addition on the crystallization kinetics and glass forming ability of Zr-(CuAg)-Al bulk metallic glass, *J. Alloy. Compd.* 772 (2019) 961–967, <https://doi.org/10.1016/j.jallcom.2018.09.055>.
- [63] M. Mohammadi Rahvard, M. Tamizifar, S.M. Ali Boutorabi, Zr–Co(Cu)–Al bulk metallic glasses with optimal glass-forming ability and their compressive properties, *Trans. Nonferrous Met. Soc. China* 28 (2018) 1543–1552.
- [64] D. Liang, X. Wei, C. Chang, J. Li, X. Wang, J. Shen, Effect of W addition on the glass forming ability and mechanical properties of Fe-based metallic glass, *J. Alloy. Compd.* 731 (2018) 1146–1150, <https://doi.org/10.1016/j.jallcom.2017.10.104>.

- [65] C. Chattopadhyay, B.S. Murty, Kinetic modification of the ‘confusion principle’ for metallic glass formation, *Scr. Mater.* 116 (2016) 7–10, <https://doi.org/10.1016/j.scriptamat.2016.01.022>.
- [66] L. Battezzati, A.L. Greer, The viscosity of liquid metals and alloys, *Acta Metall.* 37 (1989) 1791–1802, [https://doi.org/10.1016/0001-6160\(89\)90064-3](https://doi.org/10.1016/0001-6160(89)90064-3).
- [67] X.-Y. Yan, Y.A. Chang, Y. Yang, F.-Y. Xie, S.-L. Chen, F. Zhang, S. Daniel, M.-H. He, A thermodynamic approach for predicting the tendency of multicomponent metallic alloys for glass formation, *Intermetallics* 9 (2001) 535–538, [https://doi.org/10.1016/S0966-9795\(01\)00036-X](https://doi.org/10.1016/S0966-9795(01)00036-X).
- [68] C. Suryanarayana, I. Seki, A. Inoue, A critical analysis of the glass-forming ability of alloys, *J. Non. Cryst. Solids.* 355 (2009) 355–360, <https://doi.org/10.1016/j.jnoncrysol.2008.12.009>.
- [69] E. Guérin, R. Daudin, A. Lenain, N. Mendil, S. Gravier, B. Ter-Ovanesian, D. Fabregue, J.-J. Blandin, Effect of the alloy/mould contact on surface crystallisation of a biocompatible ZrCoAl bulk metallic glass, *J. Phys.: Condens. Matter* 32 (2020) 214008, , <https://doi.org/10.1088/1361-648x/ab7132>.
- [70] M. Mohammadi Rahvard, M. Tamizifar, S.M.A. Bourtoubi, Non-isothermal crystallization kinetics and fragility of Zr56Co28Al16 and Zr56Co22Cu6Al16 bulk metallic glasses, *J. Therm. Anal. Calorim.* 134 (2018) 903–914, <https://doi.org/10.1007/s10973-018-7367-8>.
- [71] M. Mohammadi Rahvard, M. Tamizifar, S.M.A. Bourtoubi, The effect of Ag addition on the non-isothermal crystallization kinetics and fragility of Zr56Co28Al16 bulk metallic glass, *J. Non. Cryst. Solids.* 481 (2018) 74–84.
- [72] W.H. Wang, Roles of minor additions in formation and properties of bulk metallic glasses, *Prog. Mater Sci.* 52 (2007) 540–596, <https://doi.org/10.1016/j.pmatsci.2006.07.003>.
- [73] P. Zhang, J.J. Maldonis, M.F. Besser, M.J. Kramer, P.M. Voyle, Medium-range structure and glass forming ability in Zr–Cu–Al bulk metallic glasses, *Acta Mater.* 109 (2016) 103–114, <https://doi.org/10.1016/j.actamat.2016.02.006>.
- [74] J. Wang, A. Agrawal, K. Flores, Are hints about glass forming ability hidden in the liquid structure? *Acta Mater.* 171 (2019) 163–169, <https://doi.org/10.1016/j.actamat.2019.04.001>.
- [75] M. Samavatian, R. Gholamipour, V. Samavatian, F. Farahani, Effects of Nb minor addition on atomic structure and glass forming ability of Zr55Cu30Ni5Al10 bulk metallic glass, *Mater. Res. Express* 6 (2019) 65202, <https://doi.org/10.1088/2053-1591/ab0bda>.
- [76] J. Zhu, M. Yang, C. Wang, S. Yang, J. Han, G. Xie, X. Liu, Formation of two-glassy-phase bulk metallic glass in Zr–Co–Al–Y immiscible system, *J. Alloy. Compd.* 781 (2019) 8–12, <https://doi.org/10.1016/j.jallcom.2018.12.005>.
- [77] J.-L. Gu, H.-W. Luan, S.-F. Zhao, H.-T. Bu, J.-J. Si, Y. Shao, K.-F. Yao, Unique energy-storage behavior related to structural heterogeneity in high-entropy metallic glass, *Mater. Sci. Eng., A* 786 (2020) 139417, , <https://doi.org/10.1016/j.msea.2020.139417>.
- [78] S. Sun, R. Ouyang, B. Zhang, T.-Y. Zhang, Data-driven discovery of formulas by symbolic regression, *MRS Bull.* 44 (2019) 559–564, <https://doi.org/10.1557/mrs.2019.156>.